Salminen, J.; Sairanen, H.; Grahn, P.; Högström, R.; Lakka, A.; Heinonen, Martti

Characterization of the Humidity Calibration Chamber by Numerical Simulations

Published in:
International Journal of Thermophysics

DOI:
10.1007/s10765-017-2221-y

Published: 01/07/2017

Document Version
Publisher's PDF, also known as Version of record

Published under the following license:
Other

Please cite the original version:
Salminen, J., Sairanen, H., Grahn, P., Högström, R., Lakka, A., & Heinonen, M. (2017). Characterization of the Humidity Calibration Chamber by Numerical Simulations. *International Journal of Thermophysics*, *38*(6), Article 84. https://doi.org/10.1007/s10765-017-2221-y

ACS OMEGA

Article

http://pubs.acs.org/journal/acsodf

Chemically Stable Atomic-Layer-Deposited Al_2O_3 Films for Processability

Mikael Broas,*[,†] Olli Kanninen,[†] Vesa Vuorinen,[†] Markku Tilli,[‡] and Mervi Paulasto-Kröckel[†]

[†]Department of Electrical Engineering and Automation, Aalto University, P.O. Box 13500, Aalto, FIN-00076 Espoo, Finland
[‡]Okmetic Oy, Piitie 2, 01510 Vantaa, Finland

Supporting Information

ABSTRACT: Atomic-layer-deposited alumina (ALD Al_2O_3) can be utilized for passivation, structural, and functional purposes in electronics. In all cases, the deposited film is usually expected to maintain chemical stability over the lifetime of the device or during processing. However, as-deposited ALD Al_2O_3 is typically amorphous with poor resistance to chemical attack by aggressive solutions employed in electronics manufacturing. Therefore, such films may not be suitable for further processing as solvent treatments could weaken the protective barrier properties of the film or dissolved material could contaminate the solvent baths, which can cause cross-contamination of a production line used to manufacture different products. On the contrary, heat-treated, crystalline ALD Al_2O_3 has shown resistance to deterioration in solutions, such as standard clean (SC) 1 and 2. In this study, ALD Al_2O_3 was deposited from four different precursor combinations and subsequently annealed either at 600, 800, or 1000 °C for 1 h. Crystalline Al_2O_3 was achieved after the 800 and 1000 °C heat treatments. The crystalline films showed apparent stability in SC-1 and HF solutions. However, ellipsometry and electron microscopy showed that a prolonged exposure (60 min) to SC-1 and HF had induced a decrease in the refractive index and nanocracks in the films annealed at 800 °C. The degradation mechanism of the unstable crystalline film and the microstructure of the film, fully stable in SC-1 and with minor reaction with HF, were studied with transmission electron microscopy. Although both crystallized films had the same alumina transition phase, the film annealed at 800 °C in N_2, with a less developed microstructure such as embedded amorphous regions and an uneven interfacial reaction layer, deteriorates at the amorphous regions and at the substrate−film interface. On the contrary, the stable film annealed at 1000 °C in N_2 had considerably less embedded amorphous regions and a uniform Al−O−Si interfacial layer.

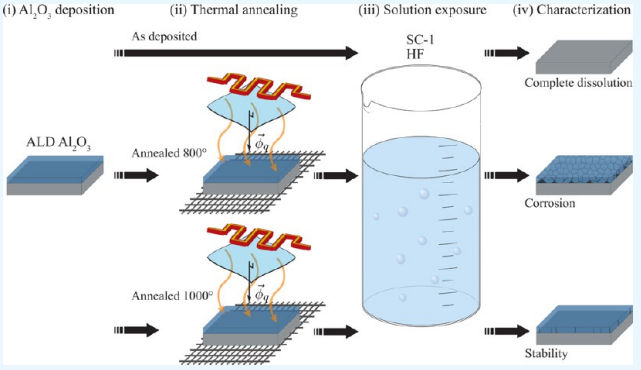

1. INTRODUCTION

Al_2O_3 deposited by atomic layer deposition (ALD) as a protective coating has attracted considerable interest in the past years.[1−4] ALD coatings in general are highly attractive due to the conformal nature of the deposited films. In principle, any geometry can be coated uniformly as long as the gaseous precursors are able to diffuse to the desired locations. Therefore, even geometries, such as pinholes and partly sealed cavities, can be protected. Protective ALD coatings can be applied in various areas such as (medical) microdevices[2,5,6] and organic electronics.[7] Besides utilizing ALD alumina films as protective coatings, they may also be used as functional and structural layers in microsystem manufacturing. For example, Al_2O_3 is known for its excellent stability as a plasma etching mask material in high-aspect-ratio micromachining.[8,9]

Al_2O_3 thin films can be exposed to various wet chemistries regardless of whether the films are utilized as protective coatings or as functional layers. Especially, the standard Radio Corporation of America (RCA) clean is highly relevant for commercial production of devices in a clean room environment.[10,11] The RCA clean is routinely applied in manufacturing to clean surfaces from contaminants. In addition to the water rinsing and drying steps, the RCA clean consists of standard clean 1 (SC-1, ammonium hydroxide and hydrogen peroxide), dilute hydrofluoric acid (HF), and standard clean 2 (SC-2, hydrochloric acid and hydrogen peroxide) solvent dips, which are all highly aggressive solutions. These solutions may deteriorate the coatings and hence either contaminate processing tools by introducing metallic contamination into the baths or decrease the barrier capability of the film. Contaminant Al on silicon wafers can cause deviation in the thermal oxidation rates of Si and fixed negative charge in the SiO_2, altering transistor performance.[12,13] Cross-contamination is an especially large concern in foundry-type manufacturing where several different products may be processed within the same facilities. Therefore, Al_2O_3 that goes through processing

Received: April 12, 2017
Accepted: June 5, 2017
Published: July 11, 2017

DOI: 10.1021/acsomega.7b00443
ACS Omega 2017, 2, 3390−3398

Table 1. Four Precursor Combinations of the ALD Al_2O_3 Films, Deposition Temperatures, and Deposition Results[a]

precursors	deposition temperature (°C)	growth per cycle (GPC) (nm/cycle)	nonuniformity (%)	thickness (nm)	refractive index
trimethylaluminum (TMA), H_2O	450	0.07	1	102	1.66
TMA, O_3	300	0.10	2	107	1.65
TMA, H_2O, O_3	300	0.10	1	103	1.65
$AlCl_3$, H_2O	450	0.07	18	89	1.65

[a]The measurements represent the average of 24 ellipsometry points from one wafer in each batch of 25 wafers. All films were visually inspected for deviations in color and obvious defects. Nonuniformities were calculated by subtracting the minimum value from the maximum and dividing by two times the average $\left(\%\ \text{nonunoformity} = \frac{\max - \min}{2 * \text{AVG}}\right)$. Negligible standard deviations (SDs) were measured for the refractive indices but the errors can be approximated to be ± 0.01.

should be fully stable and not dissolve into the cleaning baths. Furthermore, the redeposition of Al on Si has been shown to be directly proportional to the amount of contaminant Al in SC-1.[13]

ALD alumina has already displayed potential as a thin-film material with a low etch rate in a variety of solutions including SC-2;[14] however, in general, the as-deposited ALD Al_2O_3 films tend to be amorphous[15] and unstable in many solutions. For example, as-deposited ALD Al_2O_3 has been reported to be susceptible to water corrosion.[1,4,7] Nevertheless, the etch rates of ALD alumina in different solutions have distinctly varied depending on the film deposition parameters and the annealing temperature.[14] Both the deposition and the annealing temperature have been determined to be significant when fabricating chemically stable ALD alumina thin films.[1,14] The elevated temperature treatments cause the amorphous microstructure of ALD alumina to densify and to change its composition.[16] Thermal treatments at elevated temperatures lead to phase transformations of alumina and to a reduced degree of hydration.[17−19] The resulting microstructure may contribute to the chemical stability of the ALD alumina coatings. Consequently, crystalline ALD alumina films have been found resistant to H_2SO_4,[1,14,20] high-purity water,[1] KCl,[1] KOH,[1] SC-1, SC-2,[14] and other chemicals relevant in microfabrication.[14] However, none of the previous studies have analyzed in detail whether Al is nevertheless dissolved in minor quantities or whether some degree of damage is present in the films despite the films being apparently resistant to chemical attack. Furthermore, the microstructure of the stable, crystalline films has not been determined unambiguously and the deterioration mechanisms of unstable films are not comprehensively understood.

The objective of this study is to deposit and thermally treat ALD Al_2O_3 to obtain chemically stable films. The alumina films are tested in deionized water (DIW), SC-1, and HF cleaning solutions. The films are evaluated on the basis of changes in their thicknesses and refractive indices. The obtained etching rate data of soluble films may be exploited in micromachining too. The microstructures of the films are correlated with the chemical stability of the stable and unstable films. Furthermore, the degree of structural damage in the unstable films is evaluated with comprehensive scanning and transmission electron microscopy (TEM) studies. Finally, mass spectrometry (MS) is utilized to investigate the amount of solute Al contamination in the SC-1 and HF solutions.

2. RESULTS AND DISCUSSION

2.1. Al_2O_3 Films and Annealing. Al_2O_3 films were deposited from four precursor combinations. Table 1 presents information about the Al_2O_3 ALD films.

Most notably, the GPC values of the TMA-O_3- and TMA-H_2O-O_3-based films were high compared to those of the films deposited at 450 °C. The GPC of a saturated TMA-H_2O process at 300 °C has been reported to lie between 0.08 and 0.1 nm/cycle.[14,21] However, TMA begins to decompose at around 370 °C, which could, in principle, induce chemical vapor deposition type film growth.[22] However, it has been found though that the increased temperature decreases the concentration of reactive OH groups at the surface of Al_2O_3.[21] Therefore, it seems that the lower growth rate in the high-temperature processes is at least partly caused by the decreased number of reactive surface sites. Nevertheless, the GPC values and refractive indices are well in line with the previous research and comparable to those in similar processes.[14] Finally, the nonuniformity of the $AlCl_3$-based film was high and could be an issue in applications relying on strict thickness uniformity requirements.

All films presented in Table 1 underwent a thermal treatment at 1000 °C in a vacuum furnace. Furthermore, the TMA-H_2O-based films were also annealed at 600, 800, and 1000 °C in a N_2 environment. Therefore, additional rows are present in the case of TMA-H_2O in Table 2, which presents thickness and refractive index data of the annealed films. The TMA-H_2O films were selected for further characterization because the deposition behavior (Table 1), the annealing experiments (Table 2), and the etching experiments of the as-deposited films (Table 3), presented later, did not give reasons to assume that any of the other films would outperform the TMA-H_2O-based films in terms of low nonuniformity, increase in refractive index (indication of increased density[23]), and chemical stability. Furthermore, because the TMA-H_2O precursor combination is

Table 2. Thickness Decrease Data and Refractive Indices of the Alumina Films due to the Thermal Treatments[a]

sample	annealing temperature (°C)	annealing atmosphere	thickness decrease (nm)	refractive index
TMA-H_2O	1000	vacuum	6 ± 0	1.70
TMA-H_2O	1000	N_2	7 ± 0	1.70
TMA-H_2O	800	N_2	8 ± 0	1.70
TMA-H_2O	600	N_2	−3 ± 1[b]	1.65
TMA-O_3	1000	vacuum	7 ± 1	1.70
TMA-H_2O-O_3	1000	vacuum	7 ± 1	1.69
$AlCl_3$-H_2O	1000	vacuum	3 ± 9	1.69

[a]Each sample represents a complete wafer. The data were averaged from 24 ellipsometry points on each wafer. The thickness errors represent SDs (±1σ). Each film was measured before and after the thermal treatment. The refractive index errors can be approximated to be ±0.01. [b]After 600 °C annealing, the TMA-H_2O film had increased in thickness.

DOI: 10.1021/acsomega.7b00443
ACS Omega 2017, 2, 3390−3398

Table 3. Etch Rates Measured after the First Minute of Immersion in DIW at 38 °C (Vacuum-Annealed Films) and 50 °C (As-Deposited TMA-H_2O), SC-1 at 80 °C, and HF at 21 °C[a]

sample	annealing temperature (°C)	etch rate in H_2O (nm/min)	etch rate in SC-1 (nm/min)	etch rate in HF (nm/min)
TMA-H_2O	1000	0[b], -	0, 0	0
TMA-H_2O	800		0[c]	0[c]
TMA-H_2O	600		19 ± 0	19 ± 1
TMA-H_2O		0[d]	20 ± 0, 20 ± 0	24 ± 1
TMA-O_3	1000	0[b]	0	
TMA-O_3			24 ± 1	
TMA-H_2O-O_3	1000	0[b]	0	
TMA-H_2O-O_3			21 ± 1	
$AlCl_3$-H_2O	1000	0[b]	0	
$AlCl_3$-H_2O			24 ± 1	

[a]Empty space and hyphens indicate that no experiment was conducted (the etch rate columns) or that the film was in the as-deposited state (the annealing temperature column). The second reported values in the SC-1 etch rate column are from the N_2 annealing experiment encompassing also a repeated as-deposited TMA-H_2O-based film SC-1 etching experiment. All heat-treated samples used in the HF etch rate experiments were annealed in N_2. [b]The test was continued for 24 h after which the films showed a very minor thickness increase of ≤1 nm. [c]The films started to swell after 60 min. [d]The film started to swell after 15 min.

so thoroughly studied, it comes out as a more attractive precursor combination for ALD Al_2O_3 compared to the other precursor combinations in terms of being a more mature candidate for foundry-type manufacturing environments.

The thicknesses of the films decreased, except for the annealing at 600 °C in N_2, whereas the refractive indices increased, indicating compaction of the films.[14,17] The refractive index of bulk sapphire is above 1.75 at the wavelength of 632.8 nm.[24] Values similar to these values have been reported after high-temperature treatments of ALD Al_2O_3 films.[14] The large deviation in the thickness decrease of the $AlCl_3$-based film stems from the originally high nonuniformity.

The surfaces of the films were also investigated with atomic force microscopy (AFM) and optical microscopy. Figures 1 and 2 highlight the observations. The average root-mean-square (RMS) surface roughnesses of the films in the as-deposited state were 0.3−0.4 nm averaged from three locations on each film. Similar averaged RMS roughnesses were not obtained

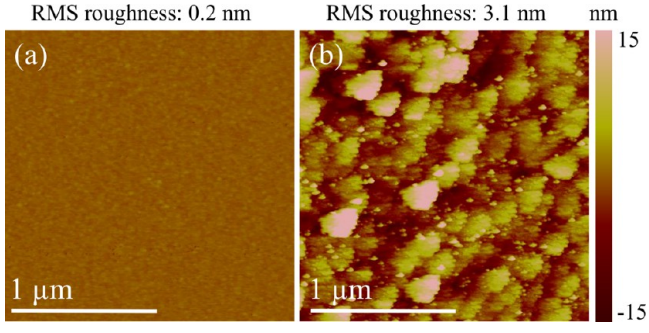

Figure 1. AFM images of (a) as-deposited and (b) 1000 °C vacuum-annealed $AlCl_3$-H_2O films from a site without a blister. The increased surface roughness is evident.

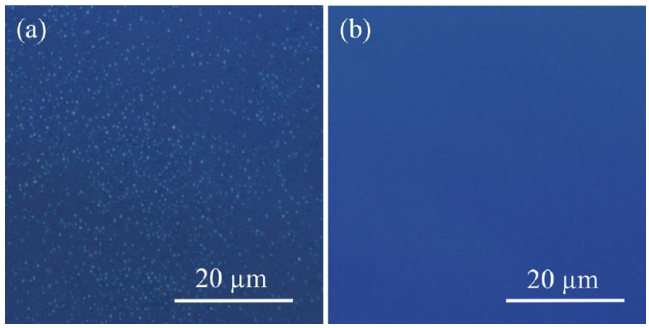

Figure 2. Optical micrographs of TMA-H_2O films annealed at 1000 °C: (a) vacuum atmosphere (the small, white dots are blisters), (b) N_2 atmosphere.

from the vacuum-annealed films because the high number of blisters (Figure 2) distorted the results. Nevertheless, the roughnesses of the films increased due to the annealing. Furthermore, as shown in Figure 2, bright circular defects, blisters, appeared on all of the films after the vacuum annealing. The optical micrographs were identical for all films with the same treatments, that is, vacuum-annealed; blistered films showed white dots and nonblistered films, including annealed and as-deposited films, displayed a deep shade of blue with no obvious defects. Blisters did not appear after the nitrogen atmosphere annealing, and the optical micrographs were identical to those of as-deposited films. Blisters have been observed in various other studies too.[25] The blisters are caused by the local delamination and subsequent bulging of the film. Stress and any gases trapped at the film−Si interface probably play a role.[25,26] Therefore, a vacuum atmosphere may exacerbate the driving force of the blister formation. Further efforts were placed on characterizing the TMA-H_2O films annealed in nitrogen because the nitrogen atmosphere annealing did not cause blistering.

2.2. Chemical Stability. The chemical stability of the films was investigated by immersing them into various solutions typically employed in wafer cleaning (DIW, SC-1, and HF). The thicknesses and refractive indices of the films were measured over regular intervals. The thickness data after 1 min of immersion were used to construct the etching rates presented in Table 3. The chip sizes were 2 × 2 cm^2. Six ellipsometry measurements were taken from each chip.

The etching data show that none of the as-deposited films would be stable during the RCA cleaning as the etch rates in SC-1 and HF are on the order of 20 nm/min. The films annealed at 1000 °C in both atmospheres and additionally the TMA-H_2O film annealed at 800 °C in N_2 seem to be stable over a short period of time of similar magnitude as in cleaning baths. The etch rates of the stable films rounded to 1 nm did not show apparent etching in SC-1 and HF after 1 min; however, the ellipsometry showed thickness decreases of some angstroms, indicating that a surface layer, such as a contaminant carbon or hydroxylated layer, had been etched.

Furthermore, prolonged exposure of 60 min to SC-1 and HF started to impose optical changes on the TMA-H_2O film annealed at 800 °C in N_2. The TMA-H_2O annealing series etching results are visualized in Figure 3, which presents the thickness change and refractive index data in graphs. The film annealed at 800 °C was not fully stable, indicated by the slight increase in thicknesses and the decrease in refractive indices

DOI: 10.1021/acsomega.7b00443
ACS Omega 2017, 2, 3390−3398

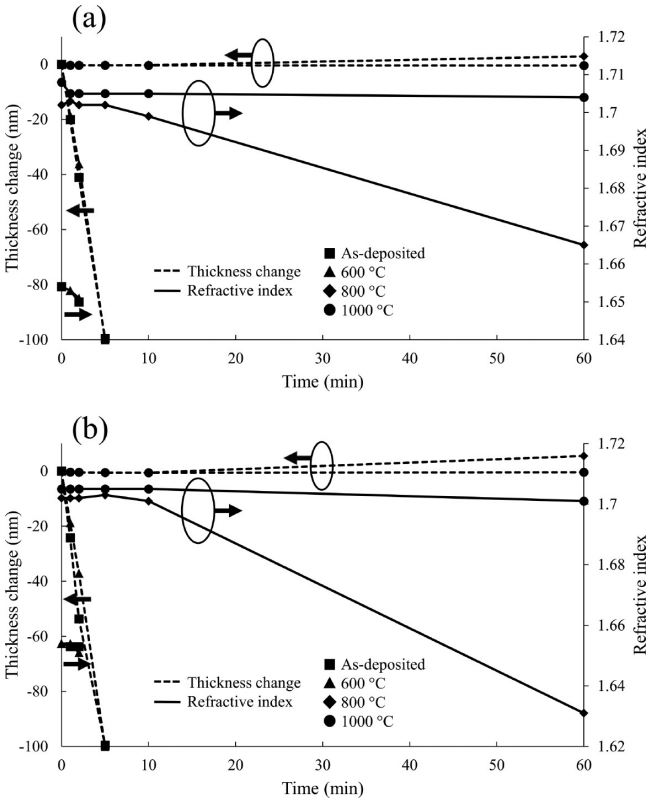

Figure 3. Changes in thicknesses and refractive indices of TMA-H_2O films as a function of immersion time in (a) SC-1 and (b) HF. The dashed lines represent the thickness changes and the solid lines represent the refractive indices. The SDs of the thickness data were on the order of maximum 1 nm. The refractive index errors can be approximated to be ±0.01. The increases in the thicknesses of the films annealed at 800 °C after 60 min were 3 and 5 nm for the SC-1 and HF treatments, respectively.

after 60 min of immersion in both SC-1 and HF. The effects are slightly more pronounced in HF.

The concentrations of the dissolved Al in the SC-1 and HF etchants were analyzed with inductively coupled plasma MS (ICP-MS). Table 4 presents these results.

Four observations can be made from the ICP-MS results. First, both as-deposited and 600 °C annealed samples showed the same concentrations of Al in the etchants as expected due to the complete dissolution of the films. Second, both reference solutions contained Al. In the case of the SC-1 experiment, some of the Al can originate from the borosilicate glass beaker where Al is a common alloying element in small quantities. However, the HF experiments were conducted in a plastic beaker. Third, the Al concentration is slightly higher, although within error limits, in HF in the 1000 °C annealed sample compared to that in the 800 °C annealed sample, which has the same concentration of the reference solution. Finally, the Al concentrations of the 800 and 1000 °C samples in SC-1 are the same as those in the reference solution. On the basis of the ICP-MS results, it may be deducted that the solubility of Al from 800 and 1000 °C N_2 annealed Al_2O_3 in SC-1 is little to none within the precision of the test setup. Both films would then be suitable for SC-1 and HF cleaning solutions.

Table 4. ICP-MS-Measured Al Concentrations in SC-1 and HF after 10 min of Etching Each Sample[a]

sample	Al concentration in SC-1 (μg/L)	Al concentration in HF (μg/L)
as-deposited	500 ± 200	400 ± 100
600 °C	500 ± 200	400 ± 100
800 °C	80 ± 20	60 ± 20
1000 °C	80 ± 20	70 ± 20
reference	80 ± 20	60 ± 20

[a]"Reference" means that the solution was kept in the beaker for 10 min without any sample. The solutions were prepared separately for each experiment. SC-1 temperature was 80 °C, and HF was at room temperature (21 °C). Chip sizes were 3 × 3 and 2 × 2 cm^2 in SC-1 and HF, respectively. The error limits represent the expanded uncertainty and were calculated with a 95% confidence interval (2σ).

2.3. Structure. The alumina films are expected to crystallize from amorphous through transition aluminas to corundum (α-Al_2O_3). The proposed temperature-dependent sequence is amorphous: → γ → δ → θ → α-Al_2O_3; however, other possibilities exist too depending on the starting material.[19] On the basis of the X-ray diffraction (XRD) results in Figure 4, the

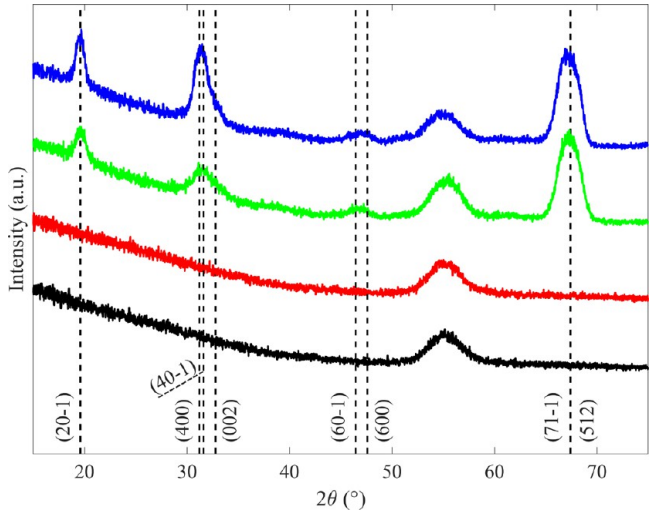

Figure 4. X-ray diffractograms of the as-deposited and N_2-annealed TMA-H_2O films. From top to bottom: 1000 °C (blue), 800 °C (green), 600 °C (red), as-deposited (black). The indexing is according to the θ-alumina diffraction data from ref 27 taken from the Inorganic Crystal Structure Database (collection code 82504).

N_2 annealing crystallized the TMA-H_2O films into the monoclinic θ-alumina at 800 and 1000 °C. The reported phase transformation temperatures of the θ phase correspond to those used in this study.[19] Another possibility, with respect to the transformation temperature, could be the κ phase, which provided a reasonable fit to the XRD data, although not as good as the θ fit (see Figure S4). The thermal treatments caused densification and increased surface roughness of the films at 800 and 1000 °C (Table 5). The films became polycrystalline with a preferred orientation because many of the strong peaks expected for an isotropically oriented powder were absent in the grazing incidence XRD (GIXRD) geometry scans (see Figure S4). The density fits of the X-ray reflectivity (XRR) at 800 and 1000 °C correspond to the reported density of the θ phase, whereas the κ phase should have a considerably higher density (3.98 g/cm^3).[19] Finally, the XRR roughness values can be seen to increase after crystallization.

TMA-H_2O-based Al_2O_3 films were imaged with scanning electron microscopy (SEM). The imaged films included the as-

DOI: 10.1021/acsomega.7b00443
ACS Omega 2017, 2, 3390−3398

Table 5. Density and Roughness Values Obtained from the XRR Measurements[a]

sample	density (g/cm^3)	surface roughness (nm)
as-deposited	3.25	0.50
600 °C	3.25	0.50
800 °C	3.55	1.30
1000 °C	3.65	1.20

[a]Error in all of the values comes mainly from the inaccuracy of the fit and is ±0.05 units.

deposited, 800 °C N_2, 1000 °C N_2, as-deposited 50 °C DIW 45 min, and 800 and 1000 °C N_2 annealed films submerged in SC-1 and HF solutions for 60 min. Figure 5 presents the most

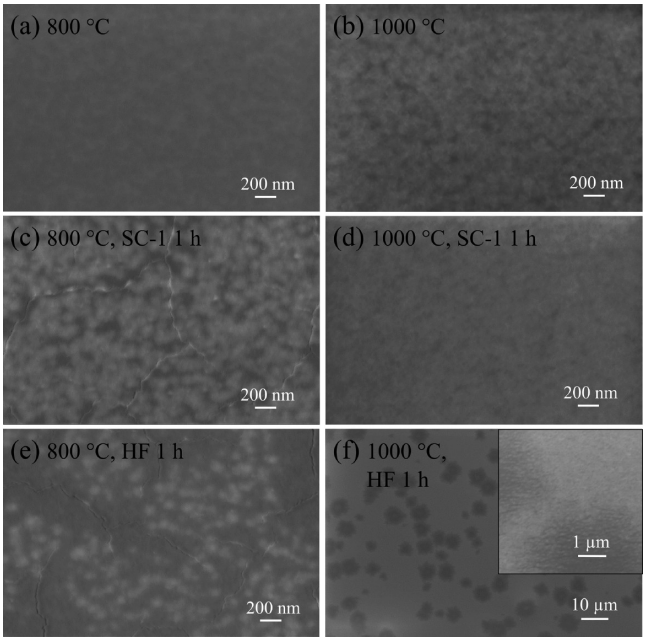

Figure 5. SEM surface micrographs of TMA-H_2O films after various treatments. The 800 °C (a) and 1000 °C (b) annealed films displayed a distinct difference in their surface morphology. The 800 °C annealed films in SC-1 (c) and HF (e) after 60 min had developed cracks and distinct differences in the surface contrast. The 1000 °C annealed films in SC-1 (d) and HF (f) after 60 min did not display cracks. The inset in (f) displays the boundary area of the two different contrast zones. Note that image (f) has a considerably different magnification compared to that of the other images to highlight the relevant observations.

important observations (as-deposited and DIW-tested film SEM images can be found in the Supporting Information). The as-deposited film was completely smooth with no observable features. The as-deposited film submerged in DIW for 45 min had developed a similar petal morphology as observed by Correa et al.[1] and Kim et al.[7] In fact, the morphology was almost fully identical to the one in the images presented by Kim et al.[7] On the basis of the ellipsometry, ICP-MS, and SEM results, the as-deposited films are not suitable for further processing that would include the full RCA clean.

The surfaces of the nitrogen atmosphere annealed films had developed features that were observable in SEM, with the morphology being rougher in the case of 1000 °C annealing. Figure 3 showed that the films annealed at 800 °C and submerged for 1 h in the SC-1 or HF had measurable changes in their thicknesses and clear changes in their refractive indices. The SEM images further revealed clear changes in these films: the films had changed surface characteristics (pronounced contrast differences) and nanocracks (Figure 5c,e). The increased contrast at the surface may originate from changes in surface topography and material density. The decrease in the refractive indices and the increase in thicknesses indicate that the films have become less dense. If the films have undergone hydroxylation or other structural changes, the films may have expanded in volume, causing cracking. ALD Al_2O_3 films tend to be in a biaxial tensile stress in their as-deposited state at room temperature.[28] Additional stress caused by the volume expansion of hydroxide products together with the internal stress of the films may be the root cause for the nanocracks. Nevertheless, it is obvious that although only small changes were observed with ellipsometry, the prolonged aggressive solvent exposure had caused structural changes in the 800 °C annealed films. On the contrary, no nanocracks, or any change in the ellipsometry data, were observed in the films annealed at 1000 °C in N_2. However, HF seems to have attacked the 1000 °C annealed film in localized areas on the surface. It is unclear whether the dark or light contrast areas, or neither, represent the original surface. It is possible that the films that have obvious contrast changes at the surface (Figure 5c,e,f) have undergone a dissolution–precipitation process theorized by Correa et al.[1] That is, the less dense surface of the films may have reacted with the solutions forming aluminum hydroxides, which have subsequently precipitated on the surfaces of the films.

The evolution of structure and the degree of damage in the films was further investigated by preparing cross-sectional TEM samples of the films in Figure 5. Figures 6–9 present the most

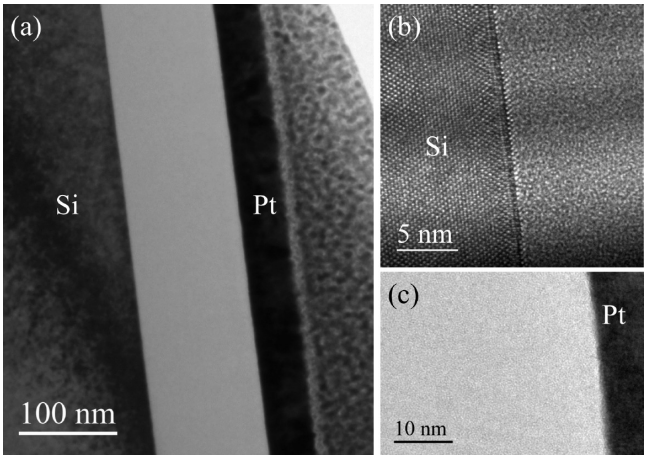

Figure 6. TEM images of the H_2O-TMA as-deposited sample. (a) Bright-field (BF) TEM taken with the smallest objective aperture selecting the zero-order beam to increase the diffraction contrast. (b) HRTEM image at the Si–Al_2O_3 interface. (c) HRTEM image at the Al_2O_3 surface. The film is clearly amorphous based on the images (a–c). No distinct phase contrast arising from a Si native oxide was seen in image (b).

relevant observations. The as-deposited TMA-H_2O film was found amorphous, as expected based on the literature (Figure 6).[15] However, the native oxide of Si was not resolved at the interface in contrast to the literature.[7,29] However, the ALD temperature was considerably higher in this study. Furthermore, TMA is known to be a highly reducing agent, which is

DOI: 10.1021/acsomega.7b00443
ACS Omega 2017, 2, 3390–3398

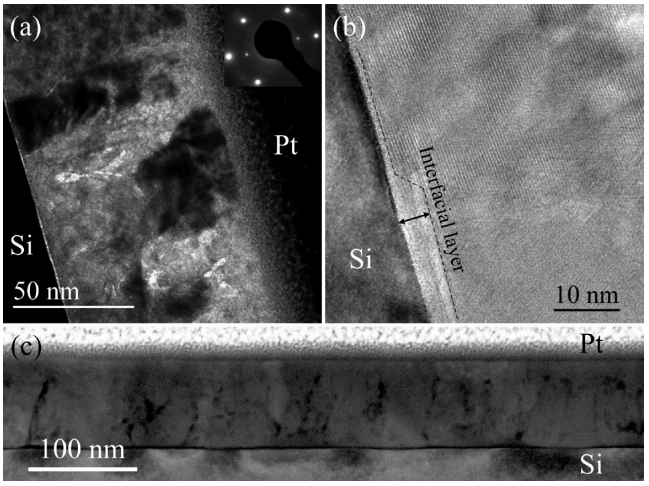

Figure 7. TEM images of the sample annealed in N_2 at 800 °C. (a) Bright-field TEM (BFTEM) overview image taken with the zero-order beam shows a polycrystalline structure. The γ value of the image has been modified to highlight the microstructure of the film. The inset shows the select-area electron diffraction (SAED) pattern along the Si$\langle 1\bar{1}0\rangle$ zone axis with only Si and Al_2O_3 selected. (b) HRTEM image at the Si–Al_2O_3 interface shows two different zones of the interfacial reaction layer. (c) Dark-field scanning TEM (DF STEM) overview image shows that the Si interface is not fully uniform and the microstructure has amorphous-like regions extending to the surface. The surface of the sample seems to have amorphized due to Ga damage, which is why no surface image was included here.

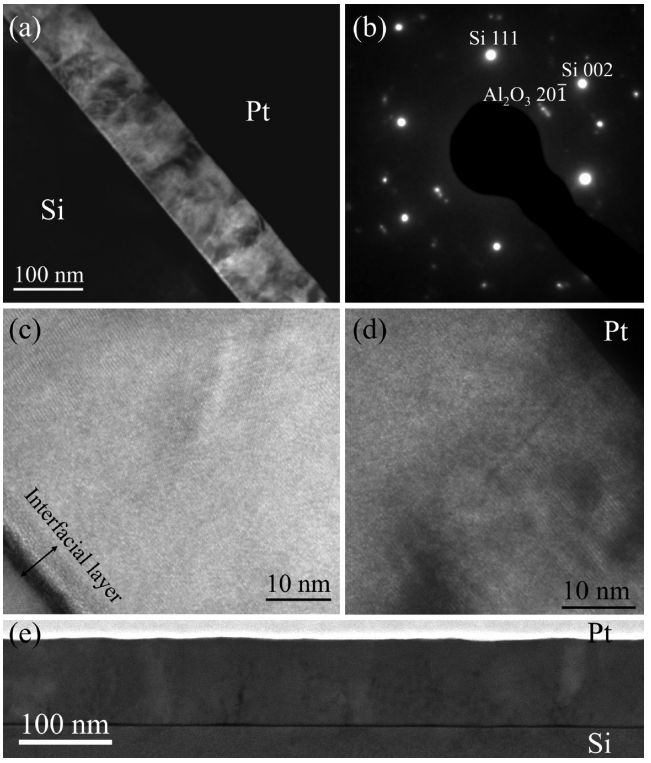

Figure 8. TEM images of the sample annealed in N_2 at 1000 °C. (a) BFTEM overview image taken with the zero-order beam shows a polycrystalline structure. The γ value of the image has been modified to highlight the microstructure of the film. (b) SAED aperture was used to select Si and Al_2O_3. The sample was oriented along the Si$\langle 1\bar{1}0\rangle$ zone axis and shows a preferential orientation for the crystallized alumina with θ-alumina (20$\bar{1}$) planes along the Si[002] direction. HRTEM images (c, d) show the Si–Al_2O_3 interface and the Al_2O_3 surface, respectively. (e) DF STEM overview image shows that the Si–Al_2O_3 interface is uniform and that little to no amorphous regions are in the film.

why it is such an effective ALD precursor too.[30] Therefore, it is possible that the native oxide has reacted during the growth, giving rise to a sharp interface between the Si substrate and the growing film, at least within the context of TEM phase contrast imaging (see Figure 6b). The Si–Al_2O_3 interface had evolved due to the annealing (Figures 6–8, Si–Al_2O_3 interfaces). Interdiffusion had taken place at the higher temperatures (i.e., at least at 800 and 1000 °C), and an Al-Si-O compound had formed between the crystalline alumina and Si (see Figure S7). The thickness of the interfacial layer has remained at sub-10 nm after 1000 °C annealing. It is noteworthy that the interfacial layer was found uniform in the sample annealed at 1000 °C with a constant thickness along the lamella, whereas the interfacial layer after 800 °C annealing did not have a constant thickness (e.g., Figure 7, high-resolution TEM (HRTEM) image where alumina lattice fringes extend to Si). Similar observations regarding the growth of interfacial layers have been made in other studies. Klie et al.[31] have shown a thin layer of SiO_2 to form during annealing when an oxygen-rich (O/Al ratio 2.1) alumina thin film was deposited on a Si substrate with no native oxide. Furthermore, Kim and Hwang[32] have shown that a thin layer of Al silicate can form between the Si substrate and the alumina film due to annealing. Finally, Zhang et al.[30] also observed an interfacial layer, whose energy-dispersive X-ray spectrometry (EDX) spectrum showed Al, O, and Si, via HRTEM to grow between the Si substrate and alumina after high-temperature annealing. In their study, the ALD alumina was crystallized on Si(111) substrates at over 1000 °C with rapid thermal annealing and showed the α-Al_2O_3(012) XRD peak. Therefore, regardless of the obtained alumina phase, it is likely that a thin reaction layer will form between the alumina film and the Si substrate. However, it is noteworthy that the excess concentration of elements beyond the stoichiometric Al_2O_3 ratio may affect the formation of the layer.

The preferential orientation of the films was investigated with SAED and HRTEM. Figures 7 and 8 show that the films annealed at 800 and 1000 °C had crystallized with a preferred orientation of stacked θ-$Al_2O_3\{20\bar{1}\}$ planes on the Si(100) surface. In the SAED patterns of Figure 7a inset and Figure 8b, the θ 20$\bar{1}$ reflections are not completely aligned with the Si 002 reflections, indicating some rotation of the preferentially oriented grains. Therefore, the GIXRD scans (i.e., nonsymmetrical XRD scans) also showed the 20$\bar{1}$ peaks as the area that is illuminated in XRD is much larger compared to that in SAED, leading to a higher probability of illuminating the highly tilted grains too. Finally, the d spacings of the 20$\bar{1}$ reflections were calculated based on the Si 002 type reflections, that is, the length measurement was calibrated with the Si unit cell, which gave a good match to the d spacing of the 20$\bar{1}$ XRD peak.

The film annealed at 800 °C and tested in SC-1 for 1 h showed bright areas extending across the film in the bright-field images (Figure 9). The bright contrast was broadened at the Si interface. These areas obviously scattered the electron beam less compared to that from the rest of film. The interfacial reaction layer was highly modified at these areas compared with the film annealed at 800 °C that had not undergone testing in SC-1 (HRTEM images of Figure 7 vs Figure 9). Furthermore, the DF STEM in Figure 9 showed similarly that the film had undergone alterations at localized points at the substrate

DOI: 10.1021/acsomega.7b00443
ACS Omega 2017, 2, 3390–3398

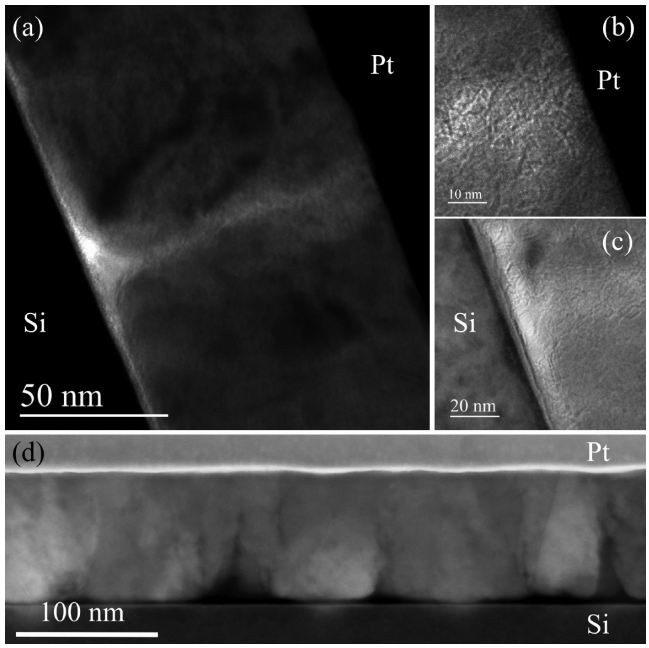

Figure 9. TEM images of the sample annealed in N_2 at 800 °C and kept in SC-1 for 60 min. (a) BFTEM image taken with the zero-order beam at a defect site shows that most of the chemical attack has taken place at the substrate interface. The γ value of the image has been modified to highlight the defect in the film. HRTEM images of the defect site at the surface (b) and the substrate interface (c). The extent of damage is evident in the DF STEM image (d).

interface with some of the areas having clear but narrow paths toward the film surface. It is reasonable to assume that the locations where a clear path toward the surface was seen correlate with the nanocracks observed in the SEM topography images. The dark areas in the DF STEM images indicate regions that scatter the electron beam less, meaning either lower Z number elements and/or lower density such as amorphous regions. Therefore, it is reasonable to assume that those areas have reacted with the SC-1 solution, resulting in an amorphous reaction product. Likewise, the HRTEM images of the SC-1-treated sample (Figure 9b,c) showed no lattice fringes in the reacted areas (both visual and fast Fourier transform inspection were used).

The film annealed at 1000 °C has more developed grains with less defects and grain boundaries compared to those in the film annealed at 800 °C. It is thermodynamically beneficial for small grains to grow, for which the increased temperature provides the kinetics. The increased density indicated by XRR also supports such notions. Furthermore, the grain boundaries themselves may have become denser and with less impurities, such as residual carbon arising from the TMA precursor during deposition, after 1000 °C annealing compared to 800 °C annealing.[33,34] Nevertheless, the most noticeable difference between the samples annealed at 800 and 1000 °C is that the number and size of the embedded amorphous regions have considerably decreased (Figure 7c vs Figure 8e). Therefore, we propose that in the 800 °C annealed film the solvents diffuse through the less stable grain boundaries/amorphous regions extending from the surface of the film to the substrate interface. The solvents then react both at the amorphous regions and at the interface. For example, Oda and Yoshio[35] have shown that the corrosion of ceramic α-Al_2O_3 mainly proceeded at the grain boundaries by the dissolution of SiO_2 and Na_2O impurities. The reaction product is less dense and will cause the refractive index to decrease although the effect on the thickness of the film is only some nanometers. The reactions inside the amorphous regions and at the interface likely also caused some volumetric increase, which in turn caused cracking visible in the SEM images; however, some of the secondary electron contrast may also come from the different density of the reacted boundaries.

3. CONCLUSIONS

ALD Al_2O_3 films were shown to be unstable in the amorphous state in DIW and SC-1, whereas heat-treated, crystalline Al_2O_3 films showed stability in DIW, SC-1, and HF. The crystalline films were realized by annealing alumina, deposited from TMA and H_2O at 450 °C, at 800 and 1000 °C. The films crystallized with a preferential orientation to the monoclinic θ-Al_2O_3 phase, where the $\{20\bar{1}\}$ planes were stacked on the (100)Si substrate. However, although the 800 °C annealed film was apparently stable according to the ellipsometry measurements during the first minutes of immersion, electron microscopy showed nanocracks on the film after 60 min of exposure to SC-1 and HF. On the contrary, the film annealed at 1000 °C was completely stable and its surface was unaffected after 60 min in SC-1, and with little modification after 60 min in HF. The deterioration of the 800 °C annealed film had taken place at embedded amorphous regions and at the substrate−film interface. The 1000 °C N_2-annealed film, fully stable in SC-1 and with minor reaction with HF, did not show dissolved Al in ICP-MS within the precision of the test setup. The films should be crystallized to process ALD Al_2O_3 in a manufacturing environment with strict requirements of purity levels. In addition, the crystalline quality needs to be sufficient (volumetric ratio of amorphous regions to crystalline regions should be minimized). Such requirements impose limitations in terms of thermal budget as the lowest possible crystallization temperature may require long annealing times to drive the crystallization of Al_2O_3 films to a sufficient fraction to preserve it from degradation. Furthermore, if the ALD Al_2O_3 is used as a barrier layer, it would be likewise beneficial to drive the grain growth to the complete thermodynamic equilibrium. Crystallization kinetics studies of ALD Al_2O_3 would provide beneficial knowledge required to fully control the grain nucleation and growth.

4. EXPERIMENTAL SECTION

4.1. ALD and Annealing. Four different precursor combinations based on TMA, $AlCl_3$, H_2O, and ozone were used in the ALD of the Al_2O_3 films. All of the films were deposited in a batch reactor (Beneq P400A) with 25 wafers in each run. The films were dual-side deposited on 150 mm single-side-polished (100)Si wafers with the native oxides. Three of the processes were binary, TMA-H_2O, TMA-O_3, and $AlCl_3$-H_2O, with alternating pulses of the metal precursor and the oxygen source. A purge cycle was applied between each step. One process, TMA-H_2O-O_3, was a ternary process without a purge sequence between the H_2O and O_3 pulses. The deposition temperatures were selected to produce as high purity films as possible and were ≥300 °C in all cases. The impurity content depends on the deposition temperature, with a higher temperature usually leading to a higher purity in the case of ALD Al_2O_3 as long as the deposition is carried out

DOI: 10.1021/acsomega.7b00443
ACS Omega 2017, 2, 3390−3398

within the process window for the particular set of precursors.[36,37]

The annealing tests were conducted in two parts. A fresh film/wafer was used in each test, that is, no film endured two sequential temperature treatments. First, all of the Al_2O_3 films were annealed for 1 h (dwell time at the maximum temperature) at 1000 °C under high vacuum (HV) conditions ($p_{tot} < 10^{-6}$ mbar) in a furnace (Webb Red Devil M). The heating ramp rate was 10 °C/min, and cooling was achieved through natural heat dissipation. Second, one of the films (precursor combinations) was selected for a set of thermal treatments based on its as-deposited quality (e.g., low nonuniformity), thermal behavior (e.g., increase in refractive index), and etching experiments (low etch rate in SC-1). The set consisted of annealing at temperatures of 600, 800, and 1000 °C for a 1 h dwell time in a N_2 environment. The N_2 environment was dictated by the furnace (PEO-603) that was used due to its higher purity classification within the research facilities. Furthermore, nitrogen is an inert gas well-suited for crystallization experiments because it is not expected to react with oxides that are more stable than the corresponding nitride compounds (e.g., Al_2O_3 vs AlN). The heating ramp rate was 15 °C/min, and the cooling rate was 13 °C/min.

4.2. Etching Experiments. The etching experiments were carried out in a fume hood inside a clean room. Borosilicate beakers (Schott Duran) were utilized in precleaning steps, DIW, and SC-1 experiments, whereas beakers made of polypropylene were used in experiments involving HF. The sample holder in all of the experiments was ethylene tetrafluoroethylene. Before the immersion into the etchant, the samples were prewashed in acetone, isopropanol, and DIW for 5 s in each solution. The etchant was kept at a desired temperature using a hot plate. The temperature of the heated etchants (i.e., not HF) was monitored using a thermometer. The samples were rinsed in DIW and dried with a nitrogen blow gun after the etching experiments.

The SC-1 solution consisted of 500 mL of DIW and 100 mL of aqueous NH_4OH (29 wt % NH_3). The liquids were mixed in a glass beaker and heated on a hot plate to a sub-target temperature. Aqueous H_2O_2 (140 mL, 30%) was added after that, and the complete solution was heated to the target temperature. The SC-1 temperature was 80 °C except when the activation energy of the etching mechanism was studied. The HF solution was prepared by mixing 500 mL of DIW and 10 mL of aqueous HF (50 wt % HF) in a plastic beaker at room temperature (21 °C). DIW experiments were conducted at 38 and 50 °C.

4.3. Thin-Film and Solvent Characterization. Ellipsometry (Plasmos SD2300) was used to measure the thicknesses and refractive indices of the films. A He−Ne laser (632.8 nm) was used as the light source. The angle of incidence was fixed to 70°.

An AFM (Digital Instruments Dimension 3100) was used to characterize the surface roughnesses of the films before and after annealing in the HV environment. Optical microscopy was used to visually inspect for defects on the films. Especially of interest were possible cracks or other similar defects after the thermal treatments. SEM (Zeiss Sigma VP) surface characterization was conducted using an in-column secondary electron detector at a 2 kV acceleration voltage.

GIXRD at the grazing angle of $\omega = 0.6°$ and XRR analyses were carried out with an X-ray diffractometer (Rigaku SmartLab) equipped with a 9 kW rotating Cu anode source. The incident beam was monochromatized using a multilayer mirror and a Ge(220) double-bounce monochromator in both the GIXRD and XRR measurements. The measured XRR curves were fitted using in-house-developed software.[38] The fitting routine was used to extract the thicknesses, densities, and roughnesses of the films. Some etched samples were selected based on the SEM characterization for further TEM inspection. The thin foil preparation was performed using focused ion beam (FIB, FEI Quanta 3D 200i and Helios NanoLab 600) systems. TEM studies were conducted at 200 kV (JEOL JEM-2800).

ICP-MS (Thermo Fisher Scientific iCAP Q) was carried out to analyze the solute Al in the SC-1 and HF solvents used to etch the films. Nitric acid (HNO_3) digestion was used in the sample preparation to assure that the aluminum in the solvents was in the ionic form. Measurements were carried out using the SFS-EN ISO 17294-2 standard.

■ ASSOCIATED CONTENT

Supporting Information

The Supporting Information is available free of charge on the ACS Publications website at DOI: 10.1021/acsomega.7b00443.

AFM images, Arrhenius plot, thickness decrease plots, XRD plots, XRR fits, SEM images of the TMA-H_2O films (as-deposited and as-deposited after 45 min in DIW), STEM-EDX maps of the TMA-H_2O film annealed at 1000 °C in N_2 (PDF)

■ AUTHOR INFORMATION

Corresponding Author

*E-mail: mikael.broas@aalto.fi.

ORCID

Mikael Broas: 0000-0002-9339-5069

Notes

The authors declare no competing financial interest.

■ ACKNOWLEDGMENTS

The research was supported by ECSEL Joint Undertaking project InForMed, grant no. 2014-2-662155. The authors would like to thank Dr. Ulla Vainio for the help with the XRD, Glenn Ross for providing the graphical abstract, and Dr. Marko Vehkamäki for the help with the FIB sample preparation. The research was conducted in the facilities of OtaNano: Micronova, Centre for Micro and Nanotechnology and the Nanomicroscopy Center, Aalto University. The ALD deposition was carried out at Beneq Oy, ICP-MS at Labtium Oy, and a part of the TEM sample preparation at the University of Helsinki.

■ REFERENCES

(1) Correa, G. C.; Bao, B.; Strandwitz, N. C. Chemical Stability of Titania and Alumina Thin Films Formed by Atomic Layer Deposition. *ACS Appl. Mater. Interfaces* **2015**, 14816−14820.

(2) Sadeghi-Tohidi, F.; Samet, D.; Graham, S.; Pierron, O. N. Comparison of the Cohesive and Delamination Fatigue Properties of Atomic-Layer-Deposited Alumina and Titania Ultrathin Protective Coatings Deposited at 200 °C. *Sci. Technol. Adv. Mater.* **2014**, *15*, No. 15003.

(3) Carcia, P. F.; McLean, R. S.; Li, Z. G.; Reilly, M. H.; Marshall, W. J. Permeability and Corrosion in ZrO2/Al2O3 Nanolaminate and Al2O3 Thin Films Grown by Atomic Layer Deposition on Polymers. *J. Vac. Sci. Technol., A* **2012**, *30*, No. 041515.

DOI: 10.1021/acsomega.7b00443
ACS Omega 2017, 2, 3390−3398

(4) Abdulagatov, A. I.; Yan, Y.; Cooper, J. R.; Zhang, Y.; Gibbs, Z. M.; Cavanagh, A. S.; Yang, R. G.; Lee, Y. C.; George, S. M. Al_2O_3 and TiO_2 Atomic Layer Deposition on Copper for Water Corrosion Resistance. *ACS Appl. Mater. Interfaces* **2011**, *3*, 4593−4601.
(5) Finch, D. S.; Oreskovic, T.; Ramadurai, K.; Herrmann, C. F.; George, S. M.; Mahajan, R. L. Biocompatibility of Atomic Layer-Deposited Alumina Thin Films. *J. Biomed. Mater. Res., Part A* **2008**, *87*, 100−106.
(6) Hoivik, N. D.; Elam, J. W.; Linderman, R. J.; Bright, V. M.; George, S. M.; Lee, Y. C. Atomic Layer Deposited Protective Coatings for Micro-Electromechanical Systems. *Sens. Actuators, A* **2003**, *103*, 100−108.
(7) Kim, L. H.; Kim, K.; Park, S.; Jeong, Y. J.; Kim, H.; Chung, D. S.; Kim, S. H.; Park, C. E. Al 2 O 3 /TiO 2 Nanolaminate Thin Film Encapsulation for Organic Thin Film Transistors via Plasma-Enhanced Atomic Layer Deposition. *ACS Appl. Mater. Interfaces* **2014**, *6*, 6731−6738.
(8) Sainiemi, L.; Franssila, S. Mask Material Effects in Cryogenic Deep Reactive Ion Etching. *J. Vac. Sci. Technol., B: Microelectron. Nanometer Struct.* **2007**, *25*, 801−807.
(9) Dekker, J.; Kolari, K.; Puurunen, R. L. Inductively Coupled Plasma Etching of Amorphous Al2O3 and TiO2 Mask Layers Grown by Atomic Layer Deposition. *J. Vac. Sci. Technol., B: Microelectron. Nanometer Struct.* **2006**, *24*, No. 2350.
(10) Kern, W. Cleaning Solutions Based on Hydrogen Peroxide for Use in Silicon Semiconductor Technology. *RCA Rev.* **1970**, *31*, 187−206.
(11) Kern, W. The Evolution of Silicon Wafer Cleaning Technology. *J. Electrochem. Soc.* **1990**, *137*, 1887−1892.
(12) Shimizu, H.; Ikeda, M.; Munakata, C.; Nagashima, N. In *Effect of Aluminum on Oxide Growth and Oxide Charges in Silicon Wafers*, Proceedings of SPIE - The International Society for Optical Engineering, 2000; pp 296−304.
(13) Lim, S. W.; Machuca, F.; Liao, H.; Chiarello, R. P.; Helms, R. C. Effect of Initial Al Contamination on Ultrathin Gate Oxides. *J. Electrochem. Soc.* **2000**, *147*, 1136−1140.
(14) Puurunen, R. L.; Saarilahti, J.; Kattelus, H. Implementing ALD Layers in MEMS Processing. *ECS Trans.* **2007**, *11*, 3−14.
(15) Miikkulainen, V.; Leskelä, M.; Ritala, M.; Puurunen, R. L. Crystallinity of Inorganic Films Grown by Atomic Layer Deposition: Overview and General Trends. *J. Appl. Phys.* **2013**, *113*, No. 021301.
(16) Jakschik, S.; Schroeder, U.; Hecht, T.; Gutsche, M.; Seidl, H.; Bartha, J. W. Crystallization Behavior of Thin ALD-Al2O3 Films. *Thin Solid Films* **2003**, *425*, 216−220.
(17) Afanas'Ev, V. V.; Stesmans, A.; Mrstik, B. J.; Zhao, C. Impact of Annealing-Induced Compaction on Electronic Properties of Atomic-Layer-Deposited Al_2O_3. *Appl. Phys. Lett.* **2002**, *81*, 1678−1680.
(18) Digne, M.; Sautet, P.; Raybaud, P.; Toulhoat, H.; Artacho, E. Structure and Stability of Aluminum Hydroxides: A Theoretical Study. *J. Phys. Chem. B* **2002**, *106*, 5155−5162.
(19) Levin, I.; Brandon, D. Metastable Alumina Polymorphs: Crystal Structures and Transition Sequences. *J. Am. Ceram. Soc.* **1998**, *81*, 1995−2012.
(20) Sammelselg, V.; Netšipailo, I.; Aidla, A.; Tarre, A.; Aarik, L.; Asari, J.; Ritslaid, P.; Aarik, J. Chemical Resistance of Thin Film Materials Based on Metal Oxides Grown by Atomic Layer Deposition. *Thin Solid Films* **2013**, *542*, 219−224.
(21) Puurunen, R. L. Surface Chemistry of Atomic Layer Deposition: A Case Study for the Trimethylaluminum/water Process. *J. Appl. Phys.* **2005**, *97*, No. 121301.
(22) Elliott, S. D.; Scarel, G.; Wiemer, C.; Fanciulli, M.; Pavia, G. Ozone-Based Atomic Layer Deposition of Alumina from TMA–Growth, Morphology, and Retention Mechanism. *Chem. Mater.* **2006**, *18*, 3764−3773.
(23) Newnham, R. E. *Properties of Materials: Anisotropy, Symmetry, Structure*; Oxford University Press on Demand: New York, 2005; pp 274−282.
(24) Malitson, I. H. Refraction and Dispersion of Synthetic Sapphire. *J. Opt. Soc. Am.* **1962**, *52*, 1377−1379.
(25) Vermang, B.; Goverde, H.; Simons, V.; De Wolf, I.; Meersschaut, J.; Tanaka, S.; John, J.; Poortmans, J.; Mertens, R. In *A Study of Blister Formation in ALD Al2O3 Grown on Silicon*, 38th IEEE Photovoltaic Specialists Conference (PVSC); IEEE, 2012; pp 1135−1138.
(26) Xie, D.-G.; Wang, Z.-J.; Sun, J.; Li, J.; Ma, E.; Shan, Z.-W. In Situ Study of the Initiation of Hydrogen Bubbles at the Aluminium Metal/oxide Interface. *Nat. Mater.* **2015**, *14*, 899−903.
(27) Husson, E.; Repelin, Y. Structural Studies of Transition Aluminas. Theta Alumina. *Eur. J. Solid State Inorg. Chem.* **1996**, *33*, 1223−1231.
(28) Ylivaara, O. M. E.; Liu, X.; Kilpi, L.; Lyytinen, J.; Schneider, D.; Laitinen, M.; Julin, J.; Ali, S.; Sintonen, S.; Berdova, M.; Haimi, E.; Sajavaara, T.; Ronkainen, H.; Lipsanen, H.; Koskinen, J.; Hannula, S. P.; Puurunen, R. L. Aluminum Oxide from Trimethylaluminum and Water by Atomic Layer Deposition: The Temperature Dependence of Residual Stress, Elastic Modulus, Hardness and Adhesion. *Thin Solid Films* **2014**, *552*, 124−135.
(29) Hoex, B.; Heil, S. B. S.; Langereis, E.; Van De Banden, M. C. M.; Kessels, W. M. M. Ultralow Surface Recombination of c-Si Substrates Passivated by Plasma-Assisted Atomic Layer Deposited Al2O3. *Appl. Phys. Lett.* **2006**, *89*, No. 042112.
(30) Zhang, L.; Jiang, H. C.; Liu, C.; Dong, J. W.; Chow, P. Annealing of Al2O3 Thin Films Prepared by Atomic Layer Deposition. *J. Phys. D.: Appl. Phys.* **2007**, *40*, 3707−3713.
(31) Klie, R. F.; Browning, N. D.; Chowdhuri, A. R.; Takoudis, C. G. Analysis of Ultrathin SiO2 Interface Layers in Chemical Vapor Deposition of Al2O3 on Si by in Situ Scanning Transmission Electron Microscopy. *Appl. Phys. Lett.* **2003**, *83*, 1187−1189.
(32) Kim, S. K.; Hwang, C. S. Atomic-Layer-Deposited Al2O3 Thin Films with Thin SiO2 Layers Grown by in Situ O3 Oxidation. *J. Appl. Phys.* **2004**, *96*, 2323−2329.
(33) Goldstein, D. N.; McCormick, Ja; George, S. M. Al2O3 Atomic Layer Deposition with Trimethylaluminum and Ozone Studied by in Situ Transmission FTIR Spectroscopy and Quadrupole Mass Spectrometry. *J. Phys. Chem. C* **2008**, *112*, 19530−19539.
(34) Broas, M.; Sippola, P.; Sajavaara, T.; Vuorinen, V.; Pyymaki Perros, A.; Lipsanen, H.; Paulasto-Kröckel, M. Structural and Chemical Analysis of Annealed Plasma-Enhanced Atomic Layer Deposition Aluminum Nitride Films. *J. Vac. Sci. Technol., A* **2016**, *34*, No. 041506.
(35) Oda, K.; Yoshio, T. Hydrothermal Corrosion of Alumina Ceramics. *J. Am. Ceram. Soc.* **1997**, *80*, 3233−3236.
(36) Matero, R.; Rahtu, A.; Ritala, M.; Leskelä, M.; Sajavaara, T. Effect of Water Dose on the Atomic Layer Deposition Rate of Oxide Thin Films. *Thin Solid Films* **2000**, *368*, 1−7.
(37) Groner, M. D.; Fabreguette, F. H.; Elam, J. W.; George, S. M. Low-Temperature Al2O3 Atomic Layer Deposition. *Chem. Mater.* **2004**, *16*, 639−645.
(38) Tiilikainen, J.; Tilli, J. M.; Bosund, V.; Mattila, M.; Hakkarainen, T.; Airaksinen, V.-M.; Lipsanen, H. Nonlinear Fitness–Space–Structure Adaptation and Principal Component Analysis in Genetic Algorithms: An Application to X-Ray Reflectivity Analysis. *J. Phys. D.: Appl. Phys.* **2006**, *40*, 215.

DOI: 10.1021/acsomega.7b00443
ACS Omega 2017, 2, 3390−3398